Morphology and Melting of Truncated Single Crystals of Linear Polyethylene

S. Hocquet,[†] M. Dosière,*[,†] A. Thierry,[‡] B. Lotz,[‡] M. H. J. Koch,[§] N. Dubreuil,[⊥] and D. A. Ivanov[⊥]

Laboratoire de Physicochimie des Polymères, Université de Mons-Hainaut, Place du Parc, 20, B-7000 Mons, Belgium; Institut Charles Sadron, rue de Boussingault, 6, F-67083 Strasbourg, France; European Molecular Biology Laboratory, Hamburg Outstation, EMBL c/o DESY, Notkestrasse 85, D-22603 Hamburg, Germany; Laboratoire de Physique des Polymères, Université Libre de Bruxelles, CP 223, Boulevard du Triomphe, B-1050 Brussels, Belgium

Received March 13, 2003; Revised Manuscript Received July 24, 2003

ABSTRACT: The thickness of (110) and (200) sectors in truncated single crystals of linear polyethylene grown from dilute *n*-octane solution at 95 °C was measured by atomic force microscopy (AFM) in tapping mode. The (110) sector was found to be 1.1 nm thicker than the (200) sector. This can be explained by a somewhat smaller tilt angle of the chains with respect to the basal plane of the crystal. The tilt of the chains in (110) and (200) sectors, obtained by electron diffraction, is 22° and 30°, respectively. This implies that the length of the stem, i.e., the length of the straight part of the chains between two consecutive folds, is identical in both sectors of the truncated single crystals. The melting of individual LPE truncated single crystals was revisited by AFM. The melting temperatures of the (200) and (110) sectors are 124.9 and 125.9 ± 0.3 °C, respectively. The lamellar thickness distribution calculated from AFM pictures clearly indicates that reorganization into thicker lamellae takes place during heating. The melting of mats of filtration of truncated LPE single crystals has also been investigated by time-resolved small-angle X-ray scattering (SAXS) and differential scanning calorimetry (DSC). The melting curve of LPE single crystals generally exhibits two endotherms. The low and the high melting temperature endotherms are characteristic of single crystals formed from dilute solution and reorganized thicker lamellae during the heating ramp, respectively. Time-resolved SAXS measurements data indicate that two populations of lamellar crystals coexist between 122 and 128 °C. The maximum value observed for the lamellar thickness of the recrystallized material is 30 nm, i.e., twice the initial lamellar thickness of single crystals obtained from dilute solution. There is good agreement between the thicknesses of the crystalline layers obtained from the SAXS data and the values calculated from the Gibbs−Thomson relationship using experimental values of the peak temperature of the two endotherms.

1. Introduction

Linear polyethylene (LPE) single crystals grown from dilute solutions are thin lamellae with lateral dimensions of several microns and thickness on the order of 10 nm.[1−4] On the basis of an electron diffraction study, Keller[3] concluded that the macromolecules forming each single crystal are folded back and forth upon themselves. In solution, LPE single crystals consist of hollow pyramids with four or six sectors.[5−9] The fold surfaces of LPE single crystals in (110) sectors formed at high and low degree of supercooling are {(314)(110)} and {(312)(110)}, respectively.[7] LPE single crystals grown from very dilute *p*-xylene solution are bounded by four (110) faces with two truncated (200) faces appearing when the concentration or the crystallization temperature are raised. The relative size of the (110) and (200) faces or the axial ratio of single crystals increases with crystallization temperature and concentration.[10−13] Lower molecular weights give rise to higher degrees of truncation.[14] Two modes of crystal collapse have been suggested:[15] (a) plastic deformation without modification of the orientation of straight chain segments; (b) flattening without any plastic deformation leading to tilting of the chains. Models for fold packing in (110) and (200) planes were developed[9] and used as a basis for packing arrangements.[16−20] The minimum fold energies for the (110) and (200) fold surfaces were estimated to be 102.5 and 95.6 erg cm^{-2}, respectively,[20] in agreement with the fold surface energy value of 93 ± 8 erg cm^{-2} obtained from thermodynamic considerations.[21] Melting temperatures of 124.5 °C for the (200) sectors and of 126.5 °C for the (110) sectors of LPE single crystals were obtained by accurate differential scanning calorimetry (DSC) coupled to electron microscopy.[22] Assuming a value of 13 nm for the crystalline thickness of (110) and (200) sectors and 414 K for the equilibrium melting temperature and 2.8 × 10^9 erg cm^{-3} for the melting heat of fully crystalline LPE, Harrison[22] estimated the surface free energies σ_e(110) and σ_e(200) from the Gibbs−Thomson relationship to be 63.8 and 72.5 erg cm^2, respectively. Note that, in contrast with the calculated values,[20] the fold surface energy of the (110) sectors appears to be lower than that of the (200) sectors. Using identical experimental techniques, Alfonso et al.[23] concluded that the multiple endotherms in the 120−131 °C range were not representative of the melting of regions with different thermodynamic stability originally present in the lamellar crystals (different crystal thicknesses, surface free energies, or lattice strains).

[†] Université de Mons-Hainaut.
[‡] Institut Charles Sadron.
[§] European Molecular Biology Laboratory, Hamburg Outstation.
[⊥] Université Libre de Bruxelles.
* Corresponding author: e-mail marcel.dosiere@umh.ac.be.

10.1021/ma034315l CCC: $25.00
Published on Web 10/07/2003

This interpretation was consistent with the observations on the temperature dependence of the peak position in SAXS patterns of LPE single crystals during heating.[24]

The mechanisms involved in the modification of the lamellar thickness of semicrystalline polymers have been largely investigated and depend on their initial morphology. The stacked lamellar morphology of linear ultrahigh molecular weight polyethylene crystallized from solution exhibits, on annealing, a doubling of the lamellar thickness not accompanied by melting.[25] The lamellar thickening during annealing of solution-grown polyethylene crystals mat could occur without melting, depending on annealing temperature and heating rate.[26,27]

A balance map of two rearrangement mechanisms against the annealing temperature was proposed for LPE single crystals: (a) gradual thickening due to a solid-state rearrangement takes place below 120 °C; (b) partial melting followed by recrystallization into thicker lamellae occurs above 126 °C; (c) the two mechanisms overlap between 120 and 126 °C.[28]

Atomic force microscopy (AFM) provides images of LPE lamellar crystals similar to those obtained by transmission electron microscope (TEM).[29] Elevation measurements with AFM are, however, much easier and more accurate than those obtained by electron microscopy. There is good agreement between the lamellar thickness of LPE single crystals determined by AFM and SAXS, with differences not exceeding 0.5 nm.[30] AFM allows direct experimental determination of the difference in thickness between (110) and (200) sectors of LPE single-crystal grown from dilute solution in *n*-octane, which ranges from 0.44 to 0.85 nm, depending on the crystallization temperature.[31]

The present paper focuses on the morphology and melting of truncated LPE single crystals using a combination of atomic force microscopy (AFM), electron microscopy (TEM), small-angle X-ray scattering (SAXS), differential scanning calorimetry (DSC), and Raman spectroscopy at low wavenumbers.

2. Experimental Section

Materials. The linear polyethylene fraction, purchased from N.I.S.T. (ref 1483), has a molecular weight of $\langle M_w \rangle = 32\,100$ and a polydispersity index of 1.15.

Sample Preparation. LPE was dissolved in *n*-octane to 0.01 wt % by heating the solution to its boiling temperature under a nitrogen atmosphere. The solution was cooled to 50 °C. Self-seeding, which allows to control the number of seeds, was applied to this solution.[32] After 30 min at the seeding temperature (107 °C), the solution was quickly transferred to the crystallization temperature. A drop of the LPE single crystals suspension was deposited either on a glass slide or on a silicon (Si) wafer. The solvent was let to evaporate at room temperature. The glass slide was further coated with a thin carbon film. Suitable areas were removed from the glass slide by flotation with poly(acrylic acid) and mounted on electron microscopy grids. The LPE crystals deposited on Si wafers were used for AFM studies. Preparation of well-oriented mats of filtration of LPE single crystals has been described elsewhere.[33]

Methods. a. Atomic Force Microscopy. Characterization of morphology and thermal behavior of single crystals of LPE was performed by AFM (Multimode AFM coupled to the Nanoscope III controller of Digital Instruments, Santa Barbara, CA) in tapping mode under dry argon. The vertical sensitivity of the scanner was calibrated with special height standards (NTMDT, Russia) chosen according to the thickness of the studied objects. The microscope is equipped with a high-temperature heater accessory,[34] controlling both the temperature of the sample and the tip. Briefly, heating of the sample to the target temperature, defined by the operator, is controlled by feedback from a thermocouple positioned under the sample, close to the sample puck. The temperature of the AFM hot stage was calibrated with phenacetin (T_m = 134.7 °C). The melting temperature of phenacetin was found to be 137.6 ± 0.3 °C. A correction of −2.9 ± 0.3 °C was therefore applied to the temperatures given by the hot stage.

The temperature of the cantilever is measured from its fundamental resonant frequency and can be adjusted by applying a voltage to a small resistive heater located inside the tip holder. Details of the AFM operation at high temperature and, in particular, methods for active control of the tip temperature have been described elsewhere.[35]

Processing and analysis of AFM images—flattening, cross-section, and histogram analyses—were performed with programs written for the purpose in Igor Pro (Wavemetrics Ltd). The routines, which make it possible to flatten AFM images by performing line-by-line or plane fits, are coupled to drawing tools, allowing operations on selected parts of the image. Advanced image processing was indispensable for accurate measurements of the crystal thickness and, especially, for discriminating between the thickness of different sectors in a single crystal.

b. Electron Diffraction. Each isolated sedimented single crystal was rotated around its crystallographic *b*-axis in the electron microscope (Philips CM12) to obtain a two-dimensional electron diffraction pattern corresponding to the *a***b** reciprocal plane. The rotation angle read on the tilting stage is a direct measure of the tilt of the chains, Φ_c. The chain tilt was also determined from the WAXD patterns of mats of filtration of LPE single crystals.[33]

c. Raman Spectroscopy. Raman spectra at low shifts (5−100 cm^{-1}) of mats of filtration of LPE single crystals were recorded with a XY800 Raman spectrometer. A triple monochromator allows to record spectra at very low wavenumbers near the Rayleigh line. A krypton−argon laser (Innova 70) delivered an incident radiation power on the filtration mats of 10−20 mW at 514 nm. The Raman spectra were recorded with a 512 channels array detector cooled with liquid nitrogen. The LAM spectra were calibrated with mats of ultralong paraffins of known lamellar thickness.[33] The wavenumber of the LAM mode is inversely proportional to the length of the chains in zigzag conformation.[36]

d. Differential Scanning Calorimetry. The melting curves of mats of filtration were obtained with a power compensated differential scanning calorimeter (Perkin-Elmer, model Pyris 1) working under a nitrogen atmosphere. Temperature and heat flow were calibrated with benzoic acid and indium for various heating rates ranging between 1 and 40 °C/min. A baseline obtained with two empty pans was subtracted from each melting curve.

e. X-ray Scattering. Time-resolved SAXS measurements were carried out on the D1/2 beamline of the EMBL in HASYLAB on the storage ring DORIS III of the Deutsches Elektronen Synchrotron (DESY) at Hamburg.[37,38] Experimental and data analysis procedures have been described elsewhere.[33]

Ni-filtered Cu Kα radiation (λ = 0.1542 nm) from a point focus rotating anode (Rigaku RU200) was used to record two-dimensional WAXD patterns of mats of filtration of single crystals on image plates with a modified Kiessig camera (pinhole collimation). Square image plates with an area of about 140 cm^2 were scanned with 50 μm resolution on a Fuji X BAS-3000 imaging analyzer yielding 12 bits intensity data. The WAXD patterns were analyzed with the "X-ray" software.[39]

3. Results and Discussion

The raw experimental results obtained on truncated LPE single crystals formed in dilute solution in *n*-octane at 95 °C will be analyzed first. Data obtained from direct

Table 1. Morphological Parameters of LPE Single Crystals ($\langle M_w \rangle$ = 32 100, p = 1.15) Crystallized from *n*-Octane at 95 °C[a]

sector	L/nm	L_{am}/nm	L_{cryst}/nm	Φ_c/deg	L_c/nm	L_{Ram}/nm	T_m/°C	σ_e/(erg cm^{-2})
(200)	12.4	2.1	10.3	30	11.9	12.6	124.9	56
(110)	13.5	2.1	11.4	22	12.1	12.6	125.9	58

[a] L is the lamellar thickness obtained from AFM measurements. L_{am} is the thickness of the amorphous regions obtained from the interface distribution function. L_{cryst} is the thickness of the crystalline regions calculated from the difference between the thicknesses of the lamella and of the amorphous layers. Φ_c is the chain tilt. L_c is the length of the chain in the crystalline regions calculated from L_{cryst}/cos Φ_c. L_{Ram} is the length of the chain obtained from the Raman spectrum at low wavenumbers. T_m is the melting temperature. σ_e is the fold surface free energy.

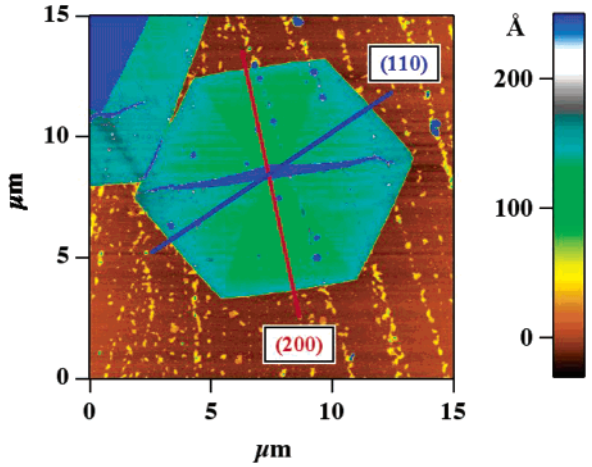

Figure 1. Tapping mode AFM image of a single crystal of linear polyethylene formed from a dilute solution in *n*-octane at 95 °C. The color code is chosen to reveal the small elevation difference between (110) and (200) crystal sectors.

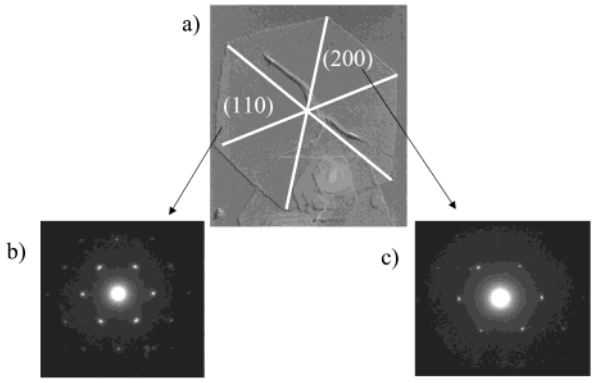

Figure 2. (a) Electron micrograph of a LPE ($\langle M_w \rangle$ = 32 100, p = 1.1) single crystal formed from a dilute solution of *n*-octane at 95 °C. (b) Electron diffraction pattern obtained at a tilt angle of 22° in a (110) sector of the single crystal shown in (a). (c) Electron diffraction pattern obtained at a tilt angle of 30° in a (200) sector of the single crystal shown in (a).

and reciprocal space techniques on similar samples are compared. AFM is the direct space technique used to image an isolated sedimented LPE single crystal at room temperature and at elevated temperatures. Time-resolved SAXS intensity curves recorded during the heating of a mat of filtration of truncated LPE single crystals through its melting represent the set of data obtained by a reciprocal space technique.

An AFM image obtained in tapping mode on a truncated LPE single crystal is shown in Figure 1. The color code is chosen to reveal the small difference between the thickness of the four (110) and two (200) sectors, which is less than 4% of the average lamellar elevation. The two (200) sectors represent 33% of the area of the single crystal. The central pleat resulting from the collapse of the pyramidal single crystal during sedimentation is oriented along the crystallographic *b*-axis.

The electron micrograph of a LPE single crystal prepared in the same conditions is given in Figure 2a. The tilt angle of the chains in the (110) and (200) sectors was estimated by rotating the single crystal around its crystallographic *b*-axis to obtain a diffraction pattern corresponding to the (*hk*0) plane (Figure 2b,c). The mean chain tilt amounts to 22° in (110) sectors and 30° in (200) sectors (Table 1).

AFM pictures of a truncated LPE single crystal successively measured at 121.9, 123.9, 124.9, and 125.9 °C are given in Figure 3. These images show that the (200) sectors melt first.

DSC curves of mats of filtration of LPE ($\langle M_w \rangle$ = 32 100) crystallized at 95 °C were recorded at various heating rates: 1, 5, 10, and 40 °C/min (Figure 4). Two endotherms are observed in the melting curves recorded at heating rates equal to and higher than 5 °C/min. A third endotherm is observed between the low- and high-temperature endotherms in the melting curve recorded at the lowest heating rate (1 °C/min).

SAXS curves were measured during heating of a mat of filtration of LPE single crystals at 5 °C/min from room temperature through its melting (Figure 5). Each SAXS curve was recorded during 20 s. Specific aspects of data analysis are considered below.

Thickness of (110) and (200) Sectors. The averaged cross-section profiles measured along the normal to the (110) and (200) growth faces of the AFM picture are given in Figure 6. They clearly illustrate that the thickness of the (110) sectors is between 0.9 and 1.3 nm larger than that of the (200) sectors. Similar results have been reported on the basis of contact mode AFM imaging of truncated LPE single crystals.[31] The AFM elevation histogram analysis (solid line in Figure 7) was performed to establish the statistical significance of our results. The histogram exhibits a maximum corresponding to the most probable crystal height at 13.5 nm along with a shoulder at 12.4 nm. For further analysis, the image was split in parts containing different crystal sectors, and the elevation histograms were separately computed for each sector. The dashed and dotted lines in Figure 7 correspond to the elevation histograms of the (200) and (110) sectors, respectively. The shoulder at low elevations in the overall histogram corresponds to the thinner (200) sectors, while the main peak reflects the elevation of the (110) sectors. The characteristic elevations of both types of sectors are given in Table 1. The height difference between the two sectors equals 1.1 nm, independent of whether the most probable or average elevation of the sectors is used. Since the integrals under the individual sector histograms represent the corresponding sector areas,

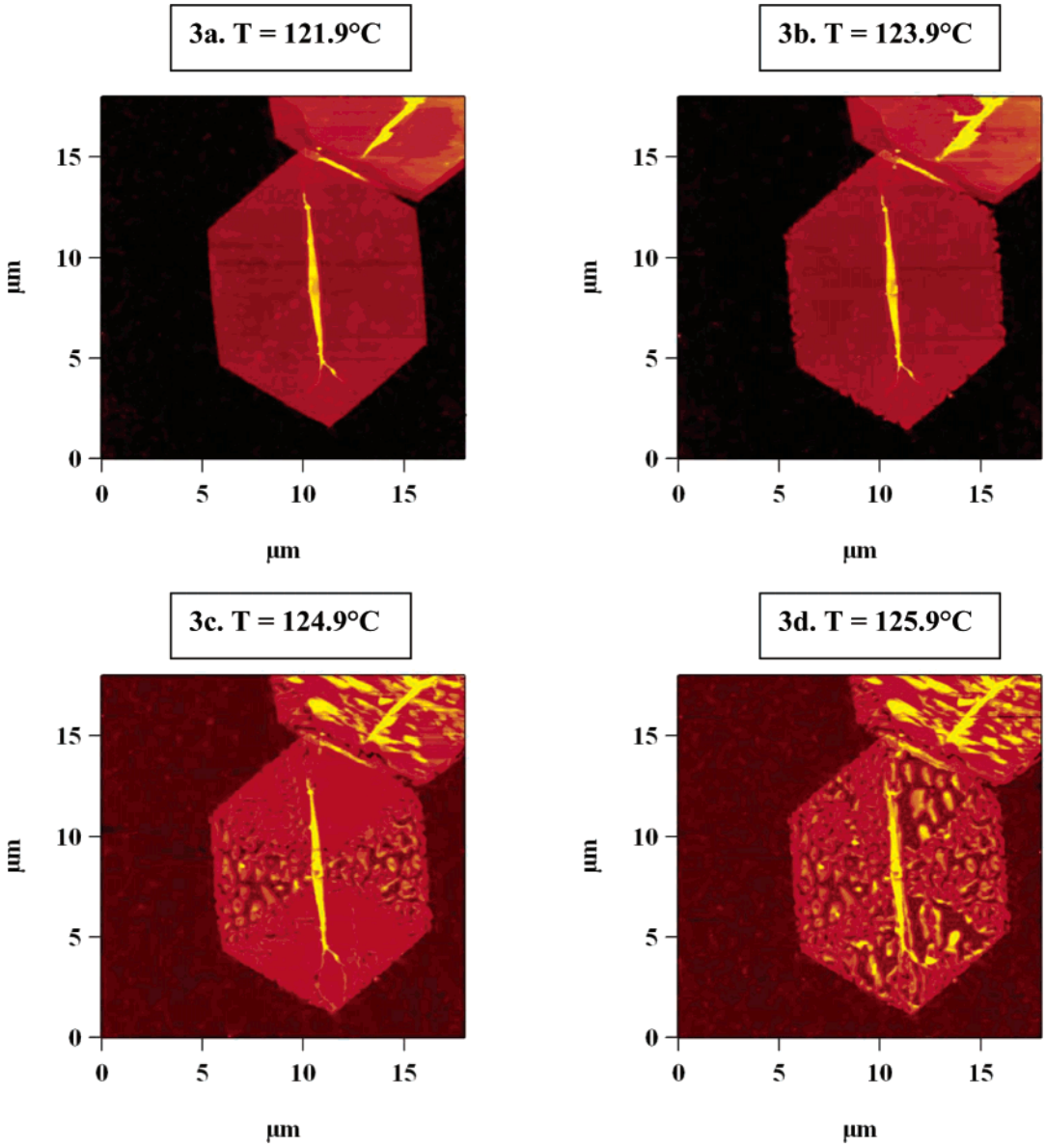

Figure 3. Tapping mode AFM images of a LPE single crystal formed from a dilute solution of *n*-octane at 95 °C taken at 121.9, 123.9, 124.9, and 125.9 °C.

they scale according to the crystal aspect ratio. The dominant (110) sectors thus determine the most probable height. Note that the accuracy of the histogram analysis critically depends on the background correction or flattening of the image. In the present case, this can be checked by analyzing the shape of the histogram peak located at zero height corresponding to the substrate surface. The standard deviation of this peak (~0.4 nm), representative of the root-mean-square roughness of the Si substrate, ensures that the small elevation difference between the crystal sectors is meaningful and does not result from undulations of the underlying substrate.

The interface distribution function (IDF) calculated from the corrected SAXS intensity curve recorded at room temperature is given in Figure 8 (solid line). It exhibits several peaks at 2.1, 11.4, and 14.0 nm, which can be assigned to the most probable thickness of the amorphous and crystalline layers and of the lamellae, respectively. The occurrence of a positive peak for L_{cryst} immediately followed by a negative peak for the lamellar thickness in the IDF precludes precise determination of the thickness of crystalline layers from the peak maximum. Indeed, the thickness of the crystalline layers recalculated from the difference between the thickness of the lamellae and the amorphous layers is 11.9 nm, which could be indicative of an error of about 0.5 nm in L_{cryst}. Since no shoulder is observed on the first positive peak of the IDF assigned to the amorphous layer thickness, the latter was assumed to be the same in both sectors. To compare AFM and SAXS results, the inverted AFM image histogram (dotted line in Figure 8) is superimposed on the SAXS interface distribution function. The AFM elevation histogram is more similar to the distribution of the lamellar thicknesses than to that of the crystal thicknesses. The fact that AFM yields values of the lamellar thickness, which are somewhat smaller (ca. 0.5 nm) than the SAXS ones, can be accounted for by local deformations in the tip−sample contact area as well as by errors due to the AFM height and/or SAXS *s*-vector calibration. The thickness determined by AFM on LPE

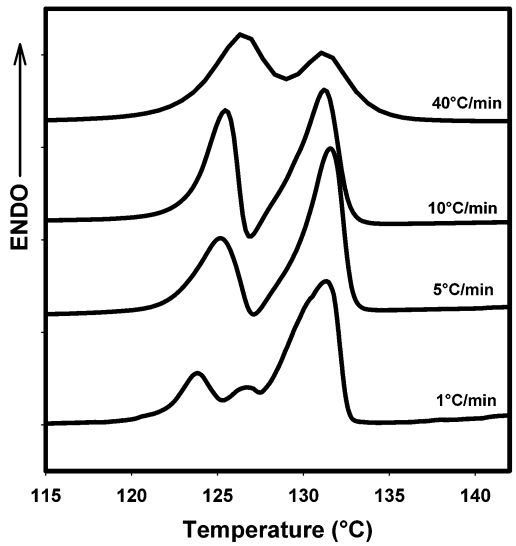

Figure 4. DSC melting curves of LPE single crystals ($\langle M_w \rangle$ = 32 100, p = 1.1) crystallized from dilute solution of *n*-octane at 95 °C obtained at heating rates 1, 5, 10, and 40 °C/min.

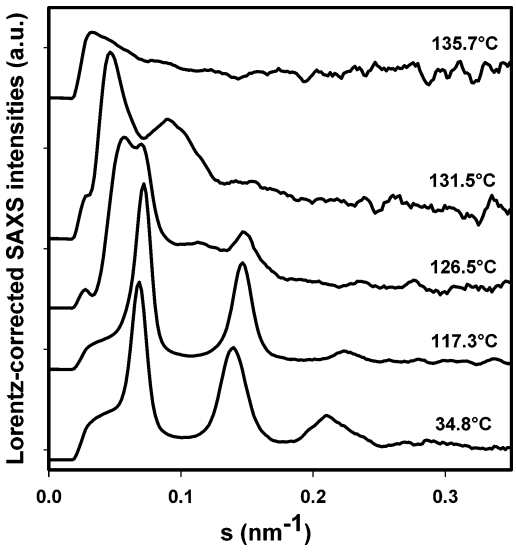

Figure 5. Time-resolved SAXS intensity curves recorded during heating of a mat of filtration of LPE single crystals ($\langle M_w \rangle$ = 32 100, p = 1.1) crystallized from dilute solution of *n*-octane at 95 °C from room temperature to 140 °C at a heating rate of 5 °C/min. Each SAXS intensity curve was recorded for 20 s.

single crystals has recently been assigned to their lamellar thickness[30] on the basis of the good agreement between the elevation measurements of lozenge-shaped LPE single crystals by AFM in tapping mode and their long spacings.

Stem Lengths in (110) and (200) Sectors. L_{cryst} values calculated by subtracting the SAXS amorphous layer thickness from the crystal height measured by AFM are equal to 11.4 and 10.3 nm in (110) and (200) sectors, respectively. The corresponding lengths L_c of the chains along the *c*-axis in the crystalline layers estimated from $L_c = L_{cryst}/\cos \Phi_c$ are equal to 12.1 and 11.9 nm in the (110) and (200) sectors, respectively. These values must be compared with the 12.6 nm found for the most probable value in the distribution of chain lengths $f(L_c)\Delta L_c$ in crystalline cores[40] (Figure 9b) calculated from the Raman spectrum at low wavenumbers (Figure 9a).

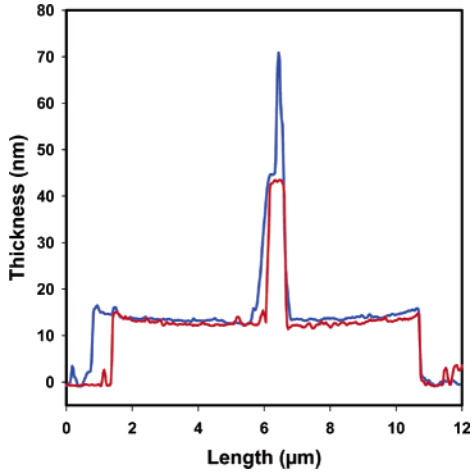

Figure 6. Elevation profiles of (110) and (200) sectors following directions perpendicular to (110) and (200) faces, respectively. The profiles of (110) and (200) sectors are given in blue and red, respectively.

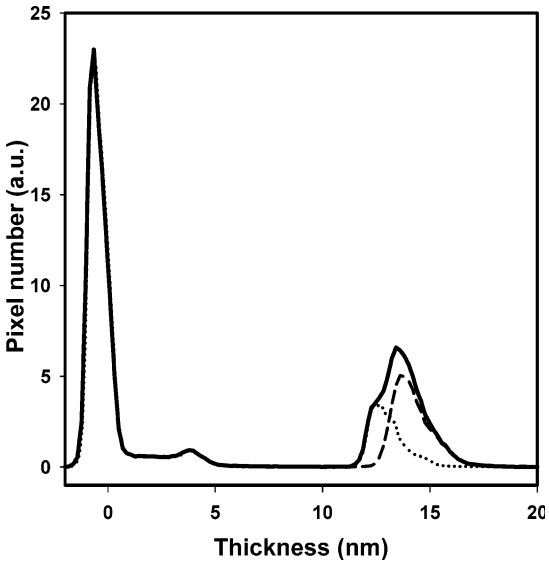

Figure 7. AFM height histograms corresponding to the image in Figure 1: histogram of the full image including four (110) and two (200) sectors (full line); histograms of the (110) sector (dotted line) and of the (200) sector (dashed line).

Melting of (110) and (200) Sectors. No trace of melting is observed in the AFM picture recorded at 121.9 °C (Figure 3a). At 123.9 °C, several cracks perpendicular to the growth faces are observed in the two (200) sectors (Figure 3b). A smaller number of similar cracks can be detected on one of the (110) faces. The (200) sectors have completely melted at 124.9 °C and recrystallized into thicker islands with an average thickness ranging between 30 and 40 nm (Figure 3c). The thickness of the recrystallized material is comparable to the height of the central pleat oriented along the crystallographic *b*-axis. Holes develop in the sectors probably due to competition between recrystallization and dewetting which follow a similar scheme in both types of sectors (Figure 3d).

This AFM investigation of the melting of a six-sector LPE single crystal confirms that (200) sectors melt at a

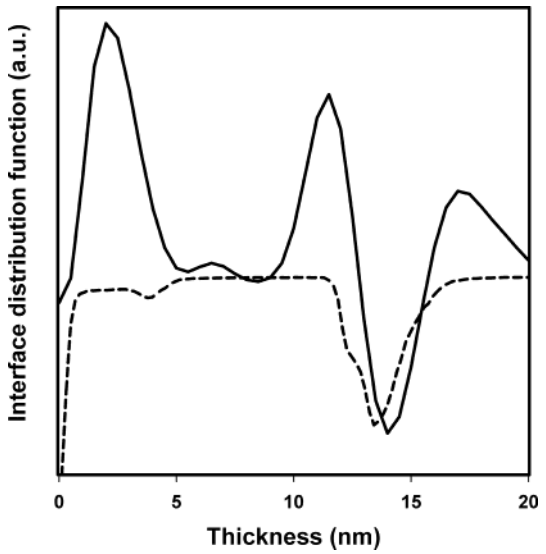

Figure 8. SAXS interface distribution function calculated from the SAXS intensity curve recorded at 34.8 °C given in Figure 5 (full line), inverted height histogram of the AFM image (Figure 1) (dashed line).

slightly lower temperature than (110) sectors. From the interface distribution function, the thickness of the crystalline layers of the (110) and (200) sectors has been estimated to be 11.4 and 10.3 nm, respectively. In the Gibbs−Thomson equation used to calculate the free enthalpy of fold surface, the melting heat and the equilibrium melting temperature are taken equal to 2.8 $\times$ 10^9 erg cm^{-3} and 414 K, respectively. Knowing the melting temperature and the thickness of the crystalline layers, the free enthalpy of fold surface σ_e was found equal to 58 and 56 erg cm^{-2} for (110) and (200) sectors, respectively (Table 1). These values are well below all previously reported values except those of Nakagawa et al.[31] obtained from a plot of the length of the stems estimated from AFM data vs the degree of supercooling (Table 2). The values of σ_e(110) and σ_e(200) obtained by Davé et al.,[20] 102.5 and 95.6 erg cm^{-2}, respectively, are approximately twice as large as ours. Their model gives values for the *a* and *b* crystallographic parameters differing by more than 10% from well-known unit cell parameters.[41] In view of this discrepancy, Davé et al.[20] considered that the chains are not folded along (200) planes in (200) sectors using a scheme proposed by Keller for the folds in the (200) sectors (Figure 10). The chains in the (200) sectors fold successively following [110], [1−10], [110], ... directions. The "mean" plane resulting from such folding of the chains in the (200) sectors would be parallel to the (200) planes although the folding plane would be parallel to (110) planes. The separation distance between two consecutive stems would be about 0.41 nm as in the (110) sectors, leading to similar values of the fold surface free enthalpy in the (200) and (110) sectors. Truncated LPE single crystals exhibit jagged (200) faces which would be a consequence of the chain folding illustrated in Figure 10. Supporting evidence for some jagging of the (200) growth faces is also suggested by the fact that the orientation of the decorating rods on LPE single crystals grown from solution is less regular in (200) than in (110) sectors, which suggests coexistence of different fold orientations in the (200) sectors.[42]

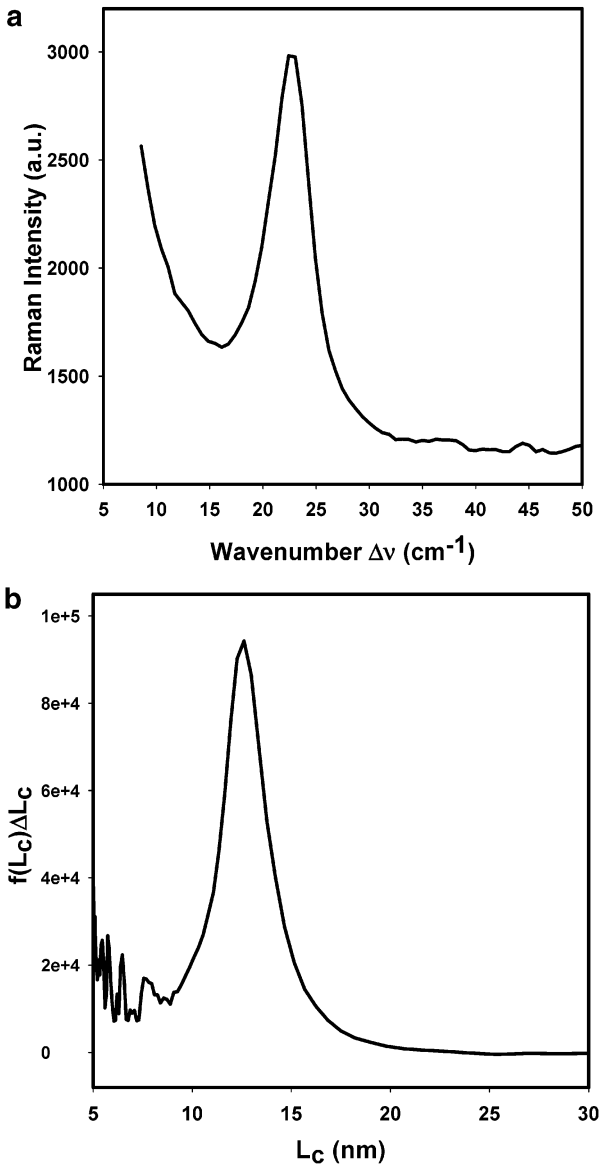

Figure 9. (a) Raman spectrum at low shift of a mat of filtration of LPE single crystals crystallized from *n*-octane at 95 °C. (b) Distribution function of chain lengths in crystalline regions $f(L_c)\Delta L_c$ vs the stem length L_c.

Table 2. Fold Surface Free Enthalpy σ_e of PE

fold surface free enthalpy σ_e/(erg cm^{-2})		
(110) sector	(200) sector	references
93 ± 8		Hoffman (1975)
93		Nakajima (1968)
63.8	72.5	Harrison (1973)
102.5	95.6	Davé (1988)
54.1	42.8	Nakagawa (1994)
58	56	this work

Time-Resolved SAXS and DSC Study of the Melting of LPE Single Crystals. Two endotherms are observed in the melting curves of mats of filtration of LPE single crystals recorded at 5 °C/min and higher heating rates (Figure 4). The peak temperature and the area under the low-temperature endotherm (I) increase with the heating rate (Figure 11). The peak temperature of the high-temperature endotherm (II) is independent

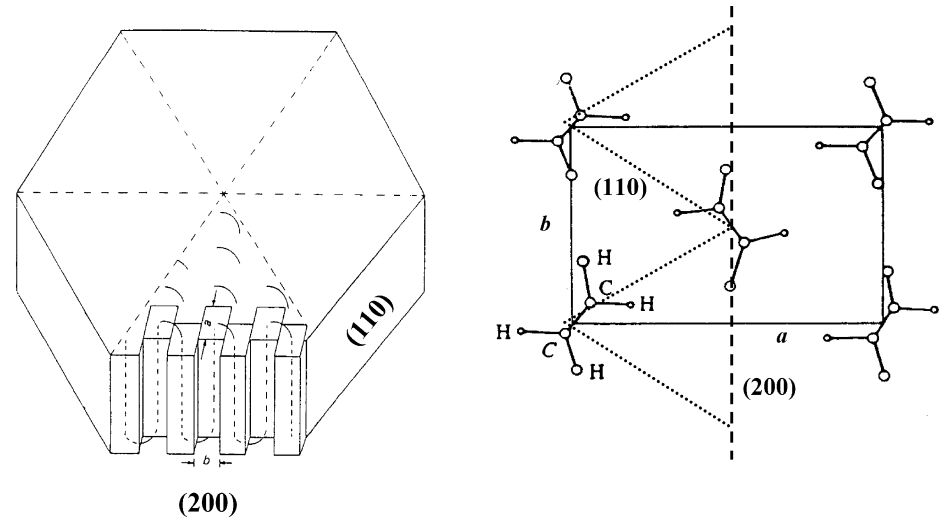

Figure 10. Schematic representation of the folds in (200) sectors: (a) three-dimensional view; (b) projection on the plane perpendicular to the chain axis: the dotted lines represent the directions of the folds.

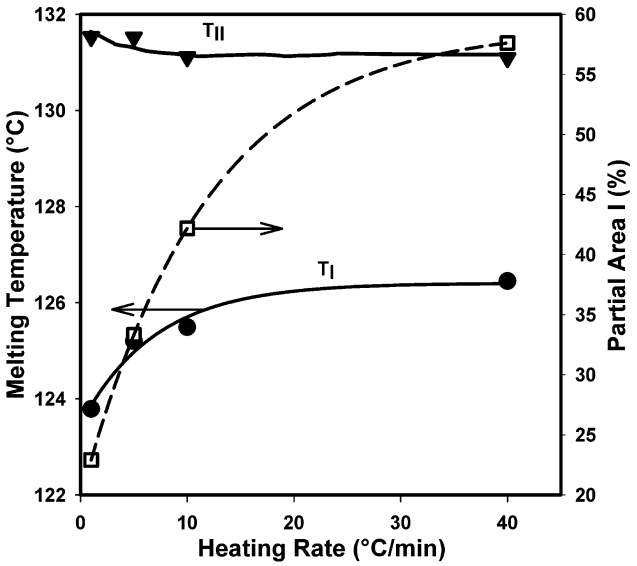

Figure 11. Peak temperatures of the melting endotherms I and II and area of the low-temperature endotherm I (%) vs heating rate.

of the heating rate, but its area decreases with increasing heating rates. A third endotherm having its extremum peaking between the endotherms I and II is observed in the melting curve recorded at 1 °C/min. These results are very similar to those reported for the same narrow molecular weight LPE fraction crystallized from dilute toluene solution.[28] The DSC analysis of mats of filtration of LPE single crystals does not allow to distinguish between the melting of (200) and (110) sectors. One reason may be due to the kind of samples investigated with the two techniques: an isolated single crystal in AFM and a "cake" with a large number of sedimented single crystals for the DSC analysis.

The melting of a mat of filtration of single crystals, heated at 5 °C/min from room temperature through its melting, has been investigated by time-resolved SAXS (Figure 5). The SAXS curves recorded between room temperature and 120 °C exhibit the first three orders of the long spacing. Careful examination of the corrected SAXS curves shows that the long spacing slightly decreases between 90 and 120 °C. From 90 through 120 °C, the magnitude of the linear decrease is around −0.013 nm/K. Similar observations have been reported from data obtained by step annealing of mats of filtration of single crystals.[24,43] It has been suggested that the decrease of the long spacing may be due to a rearrangement of the folds, resulting in a more uniform fold period and more closely packed lamellar crystals. The corrected SAXS intensity curves recorded above 120 °C clearly exhibit a shoulder which becomes finally a peak on the left side of the first order of the long spacing present at room temperature. Simultaneously with the appearance of the peak at lower *s* values, another peak develops between the first and the second orders of the initial long period. This second peak is the second order of the larger long period appearing around 122−124 °C. The SAXS intensity curves obtained above 120 °C have been fitted with Pearson function after checking that this function allows to fit correctly the three orders of the long spacing in the curves recorded between room temperature and 120 °C. The result is shown in Figure 12 for the SAXS intensity curve recorded at 125.7 °C. The second and third orders of the two long periods can be resolved for each of the two lamellar periods. Two scattering curves corresponding to each population of lamellar crystals have been simulated from the fitted curve (Figure 13a). The correlation function and the interface distribution function have been calculated from the simulated SAXS intensity curves and are given in parts b and c of Figure 13, respectively. The result of the analysis of the correlation function is given in Figure 14, illustrating the temperature dependence of the first order of the two long spacings as well as the thicknesses of the crystalline and amorphous layers of the two populations (I and II) of lamellar crystals. The numerical fit to the data indicates that the value of the lamellar thickness of the lamellae crystallized from dilute solution decreases by about 1 nm above 120 °C. The thickness of the crystalline and amorphous layers also slightly decreases. The long spacing and the thicknesses of the crystalline and amorphous layers of the crystals crystallized from the dilute solution remain

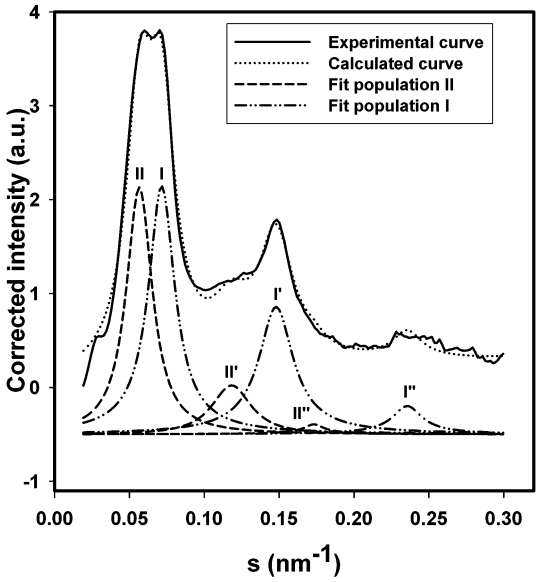

Figure 12. Corrected SAXS intensity curve recorded at 125.7 °C and various orders of the two populations of lamellar crystals obtained by fitting with a Pearson function.

constant until 127−128 °C and vanish afterward. In contrast, the long spacing and the thicknesses of the crystalline layers of the reorganized crystals in nonisothermal conditions gradually increase with temperature. An increase of 1.5 nm is observed in the thickness of the amorphous layers between 124 and 131 °C. Above this last temperature, the quality of the SAXS intensity curves is too poor for correct treatment. The thicknesses of the crystalline layers in the two lamellar populations are 10 and 18 nm, respectively. Such values are in good agreement with those calculated from the temperatures T_I and T_{II} obtained from the melting curve recorded at 5 °C/min (Figure 11) using the Gibbs−Thomson equation (10.9 and 18.3 nm).

4. Conclusions

For LPE single crystals ($\langle M_w \rangle$ = 32 100, p = 1.15) crystallized from *n*-octane at 95 °C, it was found that the lamellar thickness of the (110) sectors is about 1.1 nm larger than that of the (200) sectors. This is brought about solely by the difference in the chain tilt: the chains are more tilted in (200) than in (110) sectors as $\Phi_{c,110} = 22°$ and $\Phi_{c,200} = 30°$. Indeed, the lengths of the crystalline stems measured along the chain axis are, within experimental error, identical in both sectors. The melting temperatures of the (200) and (110) sectors determined by AFM in tapping mode are 124.9 and 125.9 °C, respectively. The free enthalpies σ_e of the fold surface in the (110) and (200) sectors have been estimated to be $\sigma_e(110) = 58$ erg/cm^2 and $\sigma_e(200) = 56$ erg/cm^2 from the Gibbs−Thomson relationship. The DSC study does not allow to identify the melting of (200) and (110) sectors of LPE single crystals.

The melting of a mat of filtration of LPE truncated single crystals was investigated by time-resolved SAXS and DSC. Above 122 °C, the SAXS curves allowed to identified two populations of lamellae. The first one consists of lamellar crystals crystallized from dilute *n*-octane solution and the second one of reorganized

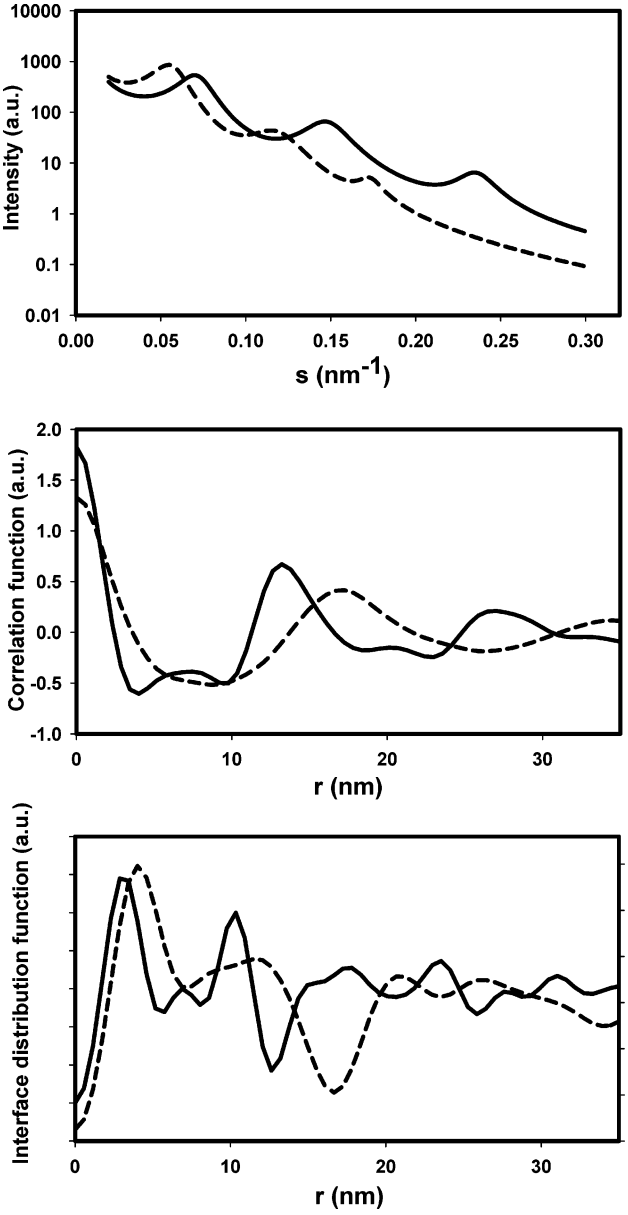

Figure 13. (a) Estimated SAXS intensity curves for the two populations (I and II) of lamellar crystals; correlation functions (b) and interface distribution functions (c) obtained for each population of lamellar crystals. I and II represent the populations of single crystals formed from dilute solution and of recrystallized material from the melt, respectively.

thicker lamellae during the scanning. The thicknesses of the crystalline and amorphous layers of this second population increase with temperature. The largest value for the lamellar thickness obtained at 132−133 °C is 28 nm, i.e., twice the value of the lamellar thickness of the isothermally crystallized single crystals from *n*-octane solution.

Acknowledgment. This work was supported by the Belgian National Fund for Scientific Research (F.N.R.S.), the European Union and the Office of Technology of the Walloon Region (Conventions 166 and 168), and the European Union through the HCMP Access to Large Installation Project, Contract HPRI-CT-1993-00017 to the EMBL. S. Hocquet acknowledges the Belgian National Fund for Scientific Research of Belgium for a PhD fellowship.

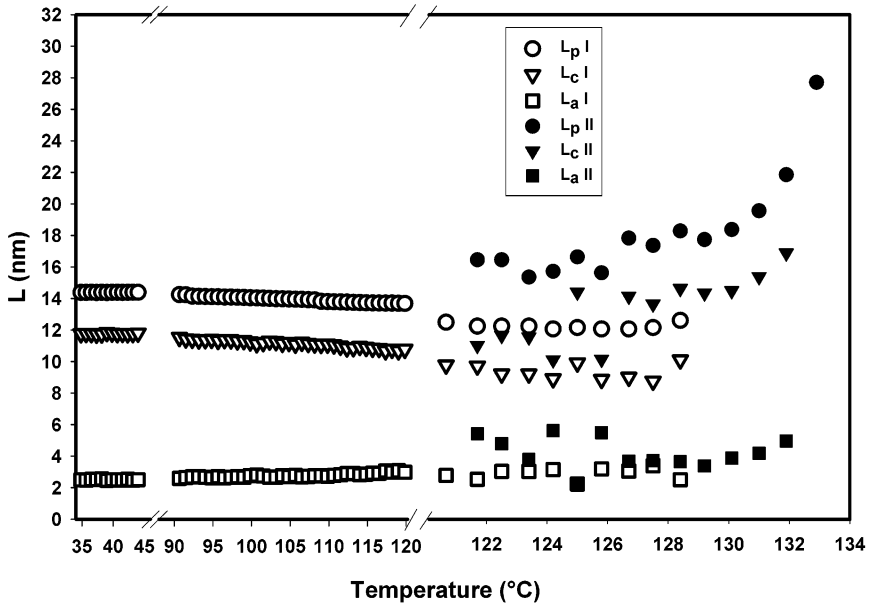

Figure 14. Thicknesses of lamellar crystals (L_p) (circles), of crystalline (L_{cryst}) (triangles), and of amorphous (L_{am}) (squares) layers vs temperature for a mat of filtration of LPE single crystals (open and filled symbols refer to populations I and II, respectively).

References and Notes

(1) Jacodine, R. *Nature (London)* **1955**, *176*, 305.
(2) Till, P. H. *J. Polym. Sci.* **1957**, *24*, 301.
(3) Keller, A. *Philos. Mag.* **1957**, *2*, 1171.
(4) Fischer, E. W. *Z. Naturforsch., A* **1957**, *12*, 753.
(5) Bassett, D. C.; Frank, F. C.; Keller, A. *Nature (London)* **1959**, *184*, 810.
(6) Bassett, D. C.; Frank, F. C.; Keller, A. *Philos. Mag.* **1963**, *8*, 1739.
(7) Bassett, D. C.; Frank, F. C.; Keller, A. *Philos. Mag.* **1963**, *8*, 1753.
(8) Niegisch, W. D.; Swan, P. R. *J. Appl. Phys.* **1960**, *31*, 1906.
(9) Reneker, D. H.; Geil, P. H. *J. Appl. Phys.*, **1960**, *31*, 1916.
(10) Keith, H. D. *J. Appl. Phys.* **1964**, *35*, 3115.
(11) Khoury, F.; Bolz, L. H. *38th Annual Proceedings of the Electron Microscopy Society of America*, San Francisco, CA, 1980; Bailey, G. W., Ed.
(12) Passaglia, E.; Khoury, F. *Polymer* **1984**, *25*, 631.
(13) Organ, S.; Keller, A. *J. Mater. Sci.* **1985**, *20*, 1571.
(14) Takamizawa, K.; Urabe, Y.; Hara, T. *Rep. Prog. Polym. Phys. Jpn.* **1969**, *12*, 179.
(15) Keller, A. *Kolloid Z. Z. Polym.* **1964**, *197*, 98.
(16) McMahon, P. E.; McCullough, R. L.; Schlegel, A. A. *J. Appl. Phys.* **1967**, *38*, 4123.
(17) Petraccone, V.; Corradini, P.; Allegra, L. *J. Polym. Sci.* **1972**, *32*, 419.
(18) Oyama, T.; Shiokawa, K.; Ishimaru, T. J. *J. Macromol. Sci., Phys.* **1973**, *8*, 229.
(19) Mazur, J.; Khoury, F.; Fanconi, B. *Bull. Am. Phys. Soc.* **1982**, *27*, 289.
(20) Davé, R. S.; Farmer, B. L. *Polymer* **1988**, *29*, 1544.
(21) Hoffman, J. D.; Davis, G. T.; Lauritzen, J. I. In *Treatise on Solid State Chemistry*; Hannay, N. B., Ed.; Plenum Press: New York, 1975; Vol. 3, Chapter 7.
(22) Harrison, I. R. *J. Polym. Sci., Polym. Phys. Ed.* **1973**, *11*, 991.
(23) Alfonso, G. C.; Ceshina, C. M.; Chiappa, V.; Pedemonte, E. In *Crystallization of Polymers*; Dosière, M., Ed.; Kluwer Academic Publishers: Dordrecht, 1993; p 455.
(24) Spells, S. J.; Hill, M. J. *Polymer* **1991**, *32*, 2716.
(25) Rastogi, S.; Spoelstra, A. B.; Goossens, J. G. P.; Lemstra, P. J. *Macromolecules* **1997**, *30*, 7880.
(26) Sadler, D. M.; Spells, S. J. *Macromolecules* **1989**, *22*, 3941.
(27) Sadler, D. M.; Spells, S. J. *Macromolecules* **1989**, *22*, 3948.
(28) Matsuda, H.; Aoike, T.; Uehara, H.; Yamanobe, T.; Komoto, T. *Polymer* **2001**, *42*, 5013.
(29) Patil, R.; Kim, S.-J.; Smith, E.; Reneker, D. H. *Polymer* **1990**, *31*, 455.
(30) Tian, M.; Loos, J. *J. Polym. Sci., Polym. Phys.* **2001**, *39*, 763.
(31) Nakagawa, Y.; Hayashi, H.; Takahagi, T.; Soeda, F.; Ishitani, A.; Toda, A.; Miyaji, H. *Jpn. J. Appl. Phys.* **1994**, *33*, 3771.
(32) Blundell, D. J.; Keller, A.; Kovacs, A. J. *J. Polym. Sci., Polym. Lett.* **1966**, *4*, 481.
(33) Hocquet, S.; Dosière, M.; Tanzawa, Y.; Koch, M. H. J. *Macromolecules* **2002**, *35*, 5025.
(34) Ivanov, D. A.; Daniels, R.; Magonov, S. "Exploring the High-Temperature AFM and Its Use for Studies of Polymers". Application Note published by Digital Instruments/Veeco Metrology Group, 2001, pp 1−12.
(35) Ivanov, D. A.; Amalou, Z.; Magonov, S. N. *Macromolecules* **2001**, *34*, 8944.
(36) Mizushima, S.; Shimanouchi, T. *J. Am. Chem. Soc.* **1949**, *71*, 1320.
(37) Koch, M. H. J.; Bordas, J. *Nucl. Instrum. Methods* **1983**, *A208*, 461.
(38) Boulin, C. F.; Kempf, R.; Gabriel, A.; Koch, M. H. J. *Nucl. Instrum. Methods* **1988**, *A269*, 312.
(39) .Information on the "X-ray" software is available on request to M. Dosière.
(40) Snyder, R. G.; Krause, S. J.; Scherrer, J. R. *J. Polym. Sci., Polym. Phys. Ed.* **1978**, *16*, 1593.
(41) Bunn, C. W. *Trans. Faraday Soc.* **1939**, *35*, 482.
(42) Wittmann, J.-C.; Lotz, B. *J. Polym. Sci., Polym. Phys. Ed.* **1985**, *23*, 205.
(43) Balta-Callega, F.; Bassett, D. C.; Keller, A. *Polymer* **1963**, *4*, 269.

MA034315L